

Strong coupling between the Eu^{2+} spins and the Fe_2As_2 layers in $\text{EuFe}_{1.9}\text{Co}_{0.1}\text{As}_2$ observed with NMR

Z. Guguchia,^{1,*} J. Roos,¹ A. Shengelaya,² S. Katrych,³ Z. Bukowski,³ S. Weyeneth,¹
F. Murányi,¹ S. Strässle,¹ A. Maisuradze,^{1,4} J. Karpinski,³ and H. Keller¹

¹Physik-Institut der Universität Zürich, Winterthurerstrasse 190, CH-8057 Zürich, Switzerland

²Department of Physics, Tbilisi State University, Chavchavadze 3, GE-0128 Tbilisi, Georgia

³Laboratory for Solid State Physics, ETH Zürich, CH-8093 Zürich, Switzerland

⁴Laboratory for Muon Spin Spectroscopy, Paul Scherrer Institute, CH-5232 Villigen PSI, Switzerland

A combination of X-ray diffraction, magnetization, and ^{75}As nuclear magnetic resonance (NMR) experiments were performed on single-crystal $\text{EuFe}_{1.9}\text{Co}_{0.1}\text{As}_2$. The strength of the hyperfine interaction between the ^{75}As nuclei and the Eu^{2+} $4f$ states suggests a strong coupling between the Eu^{2+} moments and the $\text{Fe}_{1.9}\text{Co}_{0.1}\text{As}_2$ layers. Such a strong interlayer coupling may be due to an indirect exchange interaction between the localized Eu^{2+} $4f$ moments, mediated by the Fe $3d$ conduction electrons. Magnetic susceptibility as well as ^{75}As -NMR measurements reveal a decrease of the SDW transition temperature to $T_{\text{SDW}}=120$ K as a result of Co-doping. A change of the slope in the temperature dependence of the NMR frequency of the ^{75}As lower-satellite line was observed at 225 K. At the same temperature also a change of the satellite line shape was found. These changes of the NMR spectra may be caused by the formation of a nematic phase below 225 K in $\text{EuFe}_{1.9}\text{Co}_{0.1}\text{As}_2$.

PACS numbers: 74.70.-b, 76.60.-k, 75.30.Fv, 74.25.Jb

I. INTRODUCTION

The discovery of superconductivity in iron-based arsenides at temperatures up to 56 K¹⁻⁷ has triggered extensive interest in their physical properties and the underlying mechanism of high-temperature superconductivity. The undoped parent compounds adopt a tetragonal structure at room temperature, which consists of $[\text{Fe}_2\text{As}_2]^{2-}$ layers separated by $[\text{Ln}_2\text{O}_2]^{2+}$ (Ln =lanthanoid) layers^{8,9} or A^{2+} (A =Ca, Sr, Ba, Eu) layers.¹⁰⁻¹³ At low temperatures, the parent compounds undergo a structural phase transition from a tetragonal to an orthorhombic phase, accompanied¹⁴ or followed¹⁵ by a spin density wave (SDW) transition of the itinerant Fe moments. The superconducting (SC) state can be achieved either by electron or by hole doping of the parent compounds, leading to a suppression of the SDW formation.^{6,16-18} The suppression of the magnetic transition in connection with the simultaneous formation of a SC state is reminiscent of cuprates and heavy fermion systems, therefore suggesting that the SC state in these systems is unconventional as well.

EuFe_2As_2 is a particularly interesting member of the iron arsenide $A\text{Fe}_2\text{As}_2$ ('122') family, since the A site is occupied by a Eu^{2+} S -state (orbital moment $L=0$) rare-earth ion with a $4f^7$ electronic configuration with a total electron spin $S=7/2$, corresponding to a theoretical effective magnetic moment of $7.94 \mu_B$. Figure 1 shows the crystal structure of EuFe_2As_2 . This compound is built up by $[\text{FeAs}]^{2-}$ layers, separated by layers of magnetic Eu^{2+} ions. EuFe_2As_2 exhibits both a SDW ordering of the Fe moments and an antiferromagnetic ordering of the localized Eu^{2+} moments below 190 K and 19 K, respectively. The presence of magnetic phase transitions at 19 K and 190 K in EuFe_2As_2 was seen by Mössbauer

spectroscopy¹⁹ and is confirmed by neutron diffraction.²⁰ In contrast to the other '122' systems, where the substitution of Fe by Co leads to superconductivity,^{21,22} the compounds containing Eu^{2+} exhibit the onset of a superconducting transition but seem to be hindered to reach zero resistivity at ambient pressure.²³ Reentrant superconducting behavior was also observed in a EuFe_2As_2 crystal under applied pressure up to 2.5 GPa.^{24,25} Only above 2.8 GPa a sharp resistive transition to a zero-resistivity state is achieved.²⁵ Bulk superconductivity is also observed in $\text{EuFe}_2\text{As}_{2-x}\text{P}_x$,^{26,27} where isovalent P-substitution of the As-site acts as chemical pressure on EuFe_2As_2 . No superconductivity was detected in $\text{EuFe}_{2-x}\text{Ni}_x\text{As}_2$,²⁸ while superconductivity with a maximum $T_c \simeq 20$ K was reported for $\text{BaFe}_{2-x}\text{Ni}_x\text{As}_2$.²⁹ It was suggested from different experiments^{28,30-32} that there is a strong coupling between the localized Eu^{2+} spins and the conduction electrons of the two-dimensional (2D) Fe_2As_2 layers. The study of the interaction between the rare-earth Eu^{2+} magnetic moments and the conducting Fe_2As_2 layers is important in order to understand why it is difficult to induce superconductivity in Co-doped $\text{EuFe}_{2-x}\text{Co}_x\text{As}_2$.

In order to investigate the coupling between the Eu and $\text{Fe}_{1.9}\text{Co}_{0.1}\text{As}_2$ layers as well as to study the magnetic transitions in $\text{EuFe}_{1.9}\text{Co}_{0.1}\text{As}_2$, a combination of X-ray diffraction, magnetization, and ^{75}As nuclear magnetic resonance (NMR) experiments were performed on single crystals. Magnetic susceptibility as well as ^{75}As -NMR measurements reveal a decrease of the SDW transition temperature to $T_{\text{SDW}}=120$ K for $\text{EuFe}_{1.9}\text{Co}_{0.1}\text{As}_2$. It was found that the ^{75}As NMR spectra are characterized by a negative frequency shift with respect to the ^{75}As -NMR Larmor frequency. This shift is significantly larger than the one observed in $A\text{Fe}_2\text{As}_2$ (A =Ba, Ca, Sr).³³⁻³⁶ The temperature dependence of the shift follows a Curie-Weiss type behavior with a Curie-Weiss tempera-

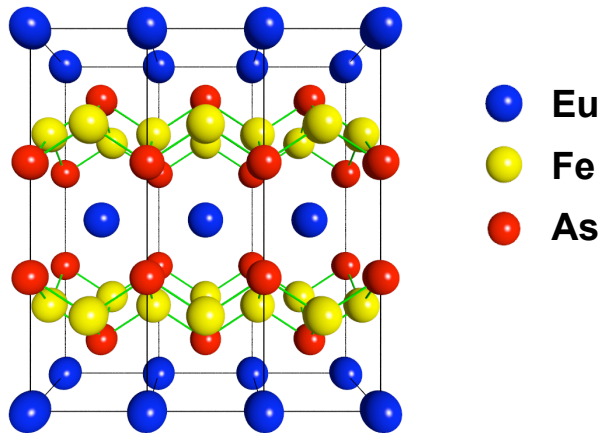


FIG. 1: (Color online) Tetragonal crystal structure of EuFe_2As_2 at room temperature, consisting of $[\text{Fe}_2\text{As}_2]^{2-}$ layers separated by Eu^{2+} layers.

ture close to the one determined from the magnetization data. The estimate of the hyperfine coupling constant between the ^{75}As nuclei and the Eu 4f states suggests a strong coupling between the Eu^{2+} magnetic moments and the $\text{Fe}_{1.9}\text{Co}_{0.1}\text{As}_2$ layers.

II. EXPERIMENTAL DETAILS

Single crystals of $\text{EuFe}_{1.9}\text{Co}_{0.1}\text{As}_2$ were grown out of Sn flux. The chemical composition of the single crystals was determined on freshly cleaved samples using wavelength-dispersive X-ray spectroscopy (WDS). The obtained composition corresponds to the formula $\text{EuFe}_{1.9}\text{Co}_{0.1}\text{As}_2$ within the experimental error ($\pm 5\%$). X-ray diffraction was performed on a single crystal of a size of approximately $0.2 \times 0.1 \times 0.008 \text{ mm}^3$ using a Bruker diffractometer equipped with the APEX II CCD detector (Bruker ASX). The data were analyzed using the APEX2³⁷ and SAINT³⁸ software. The susceptibility measurements of the crystals $\text{EuFe}_{1.9}\text{Co}_{0.1}\text{As}_2$ were carried out with a SQUID magnetometer (*QuantumDesign*) in the temperature range from 5 to 300 K in a magnetic field of 0.3 T applied parallel ($H \parallel c$) and perpendicular ($H \perp c$) to the crystallographic c -axis. The ^{75}As -NMR experiments on a single crystal (dimensions: $4 \times 4 \times 0.2 \text{ mm}^3$) from the same batch were performed in an external magnetic field of 9 T using a standard pulse spectrometer. NMR-echo signals were recorded with a frequency selective echo pulse sequence applying a phase-alternating add-subtract accumulation technique. The ^{75}As -NMR spectra were obtained by scanning the frequency in discrete steps and integrating the spin-echo signal, yielding the 'spin-echo intensity'. The spin-spin relaxation time T_2 was determined by measuring the spin-echo intensity as a function

of the delay time between the exciting and the refocusing pulse.

III. RESULTS AND DISCUSSION

A. Single crystal X-ray diffraction

X-ray diffraction experiments at room temperature revealed a good quality of the $\text{EuFe}_{1.9}\text{Co}_{0.1}\text{As}_2$ crystal. The average mosaic spread was estimated to be $\simeq 0.9^\circ$. The lattice constants for the tetragonal unit cell based upon the refinement of 689 reflections are $a = b = 3.9104(1) \text{ \AA}$, $c = 11.9434(3) \text{ \AA}$, $V = 182.629(8) \text{ \AA}^3$. The average residual for symmetry equivalent reflections is $R_{\text{int}} = 4.63\%$ and $R_\sigma = 4.01\%$. The structure was solved with XS³⁹ and subsequent structure refinements were performed with XL.⁴⁰ Because of the almost equal number of electrons, Co and Fe atoms were considered as one atom. The final anisotropic full-matrix least-squares refinement on F_0^2 with 8 variables converged at $R_1 = 2.70\%$. Further details of the structure refinement are shown in Table I. No additional phases (impurities, twins, or intergrowing crystals) were detected by examination of the reconstructed reciprocal space

TABLE I: Crystallographic and structure refinement parameters of the single crystal $\text{EuFe}_{1.9}\text{Co}_{0.1}\text{As}_2$. The diffraction study was performed at 295(2) K using MoK_α radiation with $\lambda = 0.71073 \text{ \AA}$. The lattice is tetragonal, $I4/mmm$ space group with $Z = 2$, atomic coordinates: Eu on $2a$ (0, 0, 0), Fe/Co on $4d$ (0, 1/2, 1/4), As on $4e$ (0, 0, z_{As}). A full-matrix least-squares method was employed to optimize F^2 .

Empirical formula	$\text{EuFe}_{1.9}\text{Co}_{0.1}\text{As}_2$
Unit cell dimensions (\AA)	$a = 3.9104(1)$ $c = 11.9434(3)$
Volume (\AA^3)	182.629(8)
z_{As} (atomic coordinate)	0.6388(1)
h_{pn} (\AA)	1.3286
Calculated density (g/cm^3)	7.519
Absorption coefficient (mm^{-1})	42.512
Absorption correction type	Numerical (from face indices)
$F(000)$	362
Crystal size (μm^3)	$200 \times 100 \times 8$
Theta range for data collection (deg)	3.41 to 43.92
Index ranges	$-7 \leq h \leq 5$ $-5 \leq k \leq 7$ $-22 \leq l \leq 17$
Reflections collected/unique	884/243 $R_{\text{int}} = 0.0463$
Completeness to 2Θ	97.2%
Data/restraints/parameters	243/0/8
Goodness-of-fit on F^2	1.333
Final R indices [$I > 2\text{sigma}(I)$]	$R_1 = 0.0270$ $\omega R_2 = 0.1020$
R indices (all data)	$R_1 = 0.0294$ $\omega R_2 = 0.1039$
$\Delta\rho_{\text{max}}$ and $\Delta\rho_{\text{min}}$ (e/\AA^3)	4.538 and -3.776

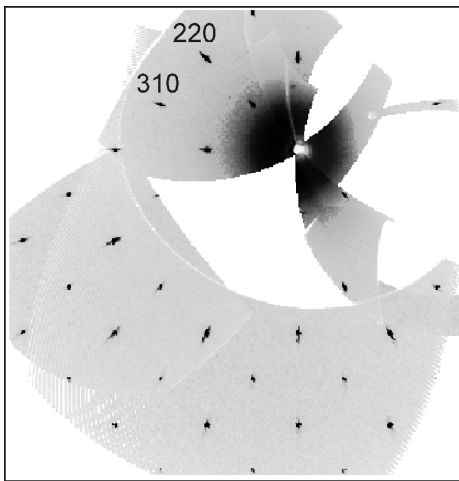


FIG. 2: (Color online) The reconstructed $hk0$ reciprocal space section of the single crystal $\text{EuFe}_{1.9}\text{Co}_{0.1}\text{As}_2$.

sections measured at room temperature (Fig. 2). In the Co-substituted crystal the room-temperature lattice parameter c is reduced and the lattice parameter a is increased relative to the parent compound EuFe_2As_2 ($a = b = 3.898(1)$ Å, $c = 12.085(5)$ Å) which was also grown out of Sn flux.

B. Magnetic Properties

Figure 3a shows the temperature dependence of the magnetic susceptibility χ for the $\text{EuFe}_{1.9}\text{Co}_{0.1}\text{As}_2$ crystal in an applied field of $\mu_0 H = 0.3$ T parallel ($H \parallel c$) and perpendicular ($H \perp c$) to the crystallographic c -axis. The temperature dependence of the inverse susceptibility for $H \perp c$ is also shown. Below 30 K, χ increases sharply, indicating ferromagnetic coupling between the Eu^{2+} moments. Below 15 K, a sudden decrease in the magnetic susceptibility for $H \perp c$ (χ_{\perp}) can be seen, indicative for a transition to the antiferromagnetic state of the Eu^{2+} moments. On the other hand, the magnetic susceptibility for $H \parallel c$ (χ_{\parallel}) remains almost constant below 15 K. This suggests that the Eu^{2+} moments align in the ab -plane,⁴¹ similar as in the case of EuFe_2As_2 .²⁰ From 50 K to 120 K, χ_{\perp} is well described by the Curie-Weiss law:

$$\chi_{\perp CW}(T) = \frac{C}{T + \Theta}. \quad (1)$$

Here C denotes the Curie-Weiss constant, and Θ the Weiss temperature. Analyzing the data with Eq.(1) in the temperature range from 30 K to 120 K yields: $C = 2.43(5) \times 10^{-4}$ m³ K/mol and $\Theta = -21.34(7)$ K. The Curie-Weiss C constant corresponds to an effective magnetic moment of $\mu_{eff} = 8.7 \mu_B$, which is slightly larger than the theoretical value of the magnetic moment of a free Eu^{2+} ion ($\mu_{free} = 7.94 \mu_B$). The negative value of Θ infers that the interaction between the Eu^{2+} moments

is ferromagnetic. Therefore, one can expect that the intralayer arrangement of the Eu^{2+} spins is ferromagnetic as in the parent compound EuFe_2As_2 . A clear drop in the susceptibility at the SDW transition temperature was observed in BaFe_2As_2 .¹⁴ In the case of EuFe_2As_2 the large signal from the Eu^{2+} spins makes it impossible to directly observe the SDW anomaly. However, after subtracting the Curie-Weiss contribution $\chi_{\perp CW}(T)$ from $\chi_{\perp}(T)$, a small anomaly in $\chi_{\perp res}(T) = \chi_{\perp}(T) - \chi_{\perp CW}(T)$ is visible at around 120 K (Fig. 3b). This behavior resembles that observed in EuFe_2As_2 ⁴² and BaFe_2As_2 ¹⁴ which was ascribed to the SDW transition of the Fe moments.

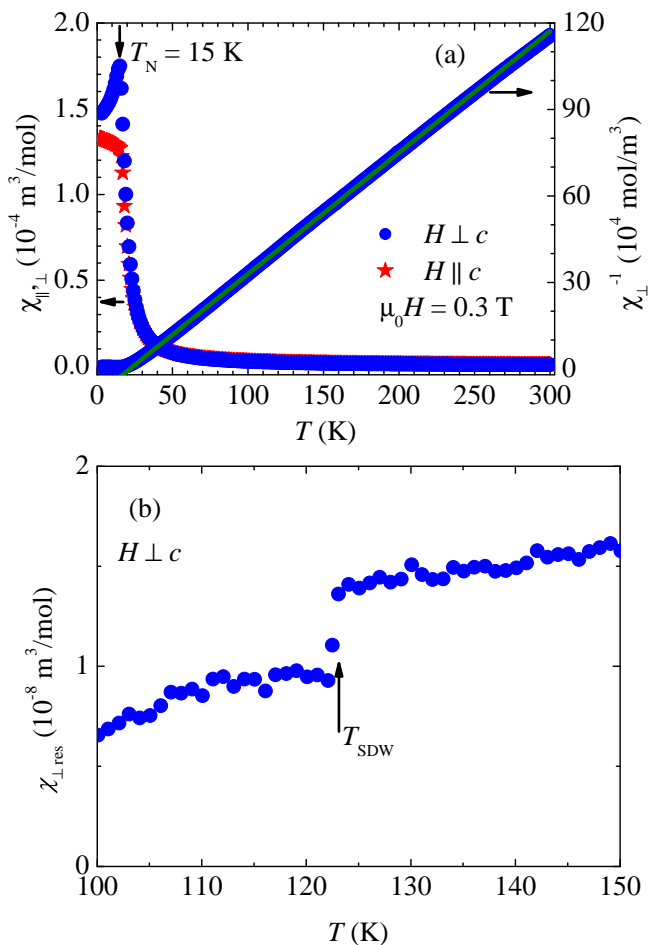


FIG. 3: (Color online) (a) Temperature dependence of the magnetic susceptibility measured in a field of $\mu_0 H = 0.3$ T applied parallel ($H \parallel c$) and perpendicular ($H \perp c$) to the crystallographic c -axis of the single crystal $\text{EuFe}_{1.9}\text{Co}_{0.1}\text{As}_2$. The measurements were performed in the zero-field cooling mode. In addition, for $H \perp c$ the temperature dependence of the inverse susceptibility $1/\chi_{\perp}$ is plotted. The solid line represents a fit to the data with the Curie-Weiss law given in Eq.(1). (b) Temperature dependence of $\chi_{\perp res}(T) = \chi_{\perp}(T) - \chi_{\perp CW}(T)$ (see text for an explanation) in the single crystal $\text{EuFe}_{1.9}\text{Co}_{0.1}\text{As}_2$.

C. Nuclear Magnetic Resonance

In this section we present ^{75}As nuclear magnetic resonance (NMR) studies in single crystal $\text{EuFe}_{1.9}\text{Co}_{0.1}\text{As}_2$. NMR is a powerful and extremely sensitive microscopic tool to probe both, magnetism and the local structure in a solid. ^{75}As has a large quadrupolar moment ($Q = 0.3b$) that interacts with the local electric field gradient (EFG) in the crystal. The nuclear spin Hamiltonian describing the interactions of the investigated nucleus with the external magnetic field and the crystal electric field gradient at the nuclear site is given by the expression:

$$H = \gamma\hbar(1 + K_\alpha)I_\alpha H_0 + \frac{h\nu_Q}{6[(3I_z^2 - 1) + \eta(I_x^2 - I_y^2)]}. \quad (2)$$

Here K_α ($\alpha = x, y, z$) is the relative magnetic shift in the α direction, I_α ($\alpha = x, y, z$) are the nuclear spin components, H_0 is the external magnetic field, γ is the gyromagnetic ratio, and ν_Q is defined as:

$$\nu_Q = \frac{3eQV_{zz}}{2I(2I - 1)\hbar} \quad (3)$$

Where V_{zz} denotes the major principal axis of the EFG tensor, and η the EFG asymmetry parameter defined as $\eta = (V_{xx} - V_{yy})/V_{zz}$ ($0 \leq \eta \leq 1$). We use the standard convention $V_{xx} \leq V_{yy} \leq V_{zz}$. Since the principal axis of the EFG tensor as well as the magnetic shift tensor are defined by the symmetry of the nuclear site, the resonance frequency of a particular nuclear transition depends on the field direction relative to the crystalline axes.

In the absence of a static magnetic field, the remaining term gives rise to double degenerate energy levels, between which nuclear quadrupole resonance (NQR) transitions can be induced. ^{75}As has a nuclear spin $I = \frac{3}{2}$ and thus two double degenerate $\pm\frac{1}{2}$ and $\pm\frac{3}{2}$ energy levels. In the presence of a large external magnetic field H_0 a splitting of the ^{75}As spectrum into a central line, arising from the central transition ($+\frac{1}{2}, -\frac{1}{2}$) and two satellite lines due to the ($\pm\frac{1}{2}, \pm\frac{3}{2}$) transitions occurs. A representative ^{75}As NMR spectrum of the central transition at 295 K is shown in the inset of Fig. 4. In the paramagnetic state ($T > T_{\text{SDW}}$) lines with a full width at half maximum (FWHM) of about 250 kHz (central line) and 500 kHz (satellite lines) are observed. Figure 4 presents the dependence of the ^{75}As -NMR central line position on the angle θ between the magnetic field orientation and the c -axis at 261 K (tetragonal phase). For all orientations of the magnetic field with respect to the c -axis the line positions show a strong negative shift relative to the corresponding ^{75}As Larmor frequency of 65.9 MHz at 9 T. ^{75}As has four nearest neighbor Fe atoms, and lies just above or below the Fe plane (see Fig. 1). In the tetragonal phase its site symmetry requires uniaxial symmetry along the c axis for the EFG tensor ($\eta = 0$) and the K tensor. The analysis of the angular dependence of the frequency of the central line using the diagonalization of

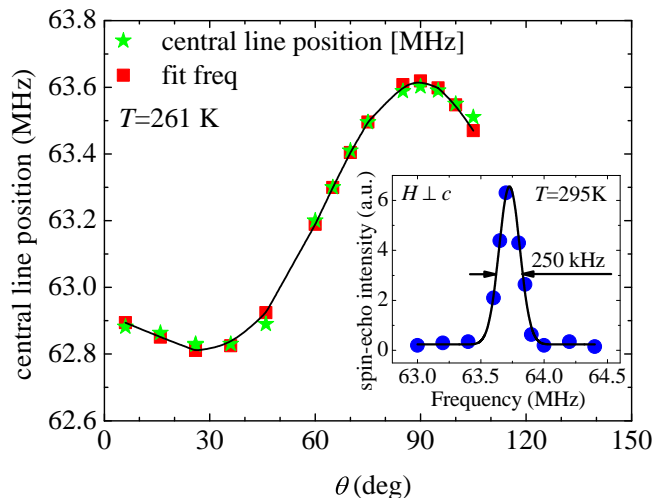


FIG. 4: (Color online) Dependence of the ^{75}As NMR central line frequency at 261 K on the angle θ between the external magnetic field and the crystallographic c -axis of single crystal $\text{EuFe}_{1.9}\text{Co}_{0.1}\text{As}_2$. The solid line is a guide to the eye. Solid squares represent the calculated frequencies as described in the text. The inset illustrates the ^{75}As NMR central line shape at 295 K. The solid line represents a Gaussian fit.

the Hamiltonian [Eq. (2)] yields $K_{ab} = -0.0372(2)$, $K_c = -0.0456(3)$, and $\nu_Q = 7.39(24)$ MHz with η set to be zero.

Figure 5a shows the temperature dependence of the spin-spin relaxation rate $1/T_2$ of the central line of the ^{75}As NMR spectrum for $H \parallel c$. $1/T_2$ exhibits a Curie-Weiss-like temperature dependence down to 120 K. This shows that the ^{75}As nuclei interact with the localized Eu- $4f$ moments. A reduction of $1/T_2$ is observed at 120 K, which reflects the slowing down of the Fe spin fluctuations due to the SDW ordering of the Fe moments. A similar behavior across the SDW transition was also reported for spin-lattice relaxation measurements in $A\text{Fe}_2\text{As}_2$ ($A = \text{Ba}, \text{Ca}, \text{Sr}$).³³⁻³⁵ However, in contrast to these findings, in our case $1/T_2$ increases again upon further cooling. This increase reflects the dominant Eu^{2+} contribution in the spin-spin relaxation process. The SDW transition below 120 K is also reflected in the temperature dependence of the NMR linewidth as shown in Fig. 5b. In addition, we observed a so-called wipeout phenomenon of the central line intensity with decreasing the temperature across the SDW transition. The temperature dependence of the wipeout fraction, defined as $F = [A_1(295 \text{ K}) - A_1(T)]/A_1(295 \text{ K})$ is displayed in the inset of Fig. 5b. The wipeout fraction is a measure for an unobserved signal intensity,^{43,44} $A_1 = I \cdot T$, where I represents the NMR echo intensity, corrected for the T_2 echo decay and integrated over the full central line. A sudden increase in the wipeout fraction and a pronounced broadening (Fig. 5b) of the ^{75}As central line can be clearly seen below 120 K. The decrease of $1/T_2$, the pronounced broadening of the ^{75}As central line, and the sudden jump of the wipeout fraction are caused by the appearance of inhomogeneous

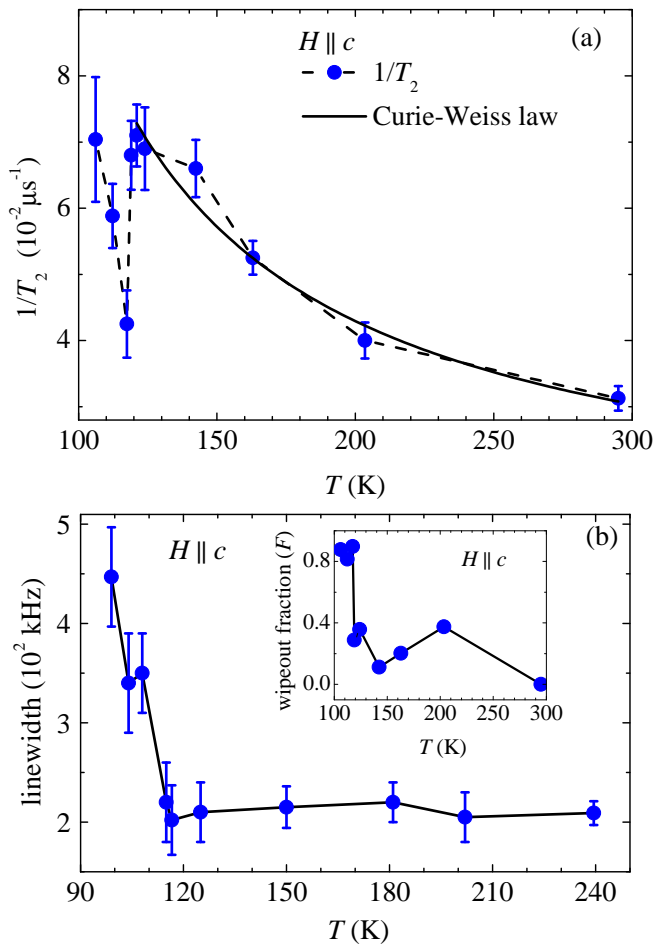


FIG. 5: (Color online) (a) Temperature dependence of the spin-spin relaxation rate $1/T_2$ of the ^{75}As central line of the single crystal $\text{EuFe}_{1.9}\text{Co}_{0.1}\text{As}_2$ for $H \parallel c$. The solid line represents the Curie-Weiss law, and the dashed line is to guide to the eye. (b) Temperature dependence of the linewidth (FWHM) and the wipeout fraction F (inset) for $H \parallel c$. Solid lines are guides to the eye.

internal magnetic fields in the SDW phase.

Next we describe the determination of the hyperfine coupling strength between the ^{75}As nuclei and Eu^{2+} $4f$ moments. For this reason we measured the temperature dependence of the magnetic shift K of the central line of the ^{75}As NMR spectrum. Since for this temperature range ν_Q is almost constant, as it will be shown below and η is very close to zero, the observed temperature dependence of the central line frequency is fully determined by the temperature behavior of K . In Fig. 6a we present the temperature dependence of the shift K in the temperature range from 100 and 300 K for $H \parallel c$ ($K_{\parallel}=K_c$) and $H \perp c$ ($K_{\perp}=K_{ab}$). Compared to the magnetic shift data for AFe_2As_2 ($A=\text{Ba}, \text{Ca}, \text{Sr}$),^{33–36} our observed shifts are significantly larger, negative, and show a completely different temperature dependence. The temperature dependence of the relative magnetic shift K above 117 K

is well described by a Curie-Weiss like behavior for both directions of the magnetic field H :

$$K(T) = K_0 + \frac{C_K}{T + \Theta}. \quad (4)$$

The inset of Fig. 6a presents the inverse of the temperature dependent part of the shift for $H \perp c$ as a function of temperature. Below the SDW transition $T_{\text{SDW}} = 120$ K the data deviates from the Curie-Weiss behavior. This deviation can be understood when considering that above T_{SDW} both the Eu and Fe sublattices are in the paramagnetic state, and both contribute to the shift, while below T_{SDW} only the Eu^{2+} moments contribute. An analysis of the data for $H \perp c$ using Eq. (4) yields: $\Theta = -18.9(9)$ K, $K_0 = 0.17(25)$ %. The value of Θ is in fair agreement with the value $\Theta = -21.34(7)$ K determined from

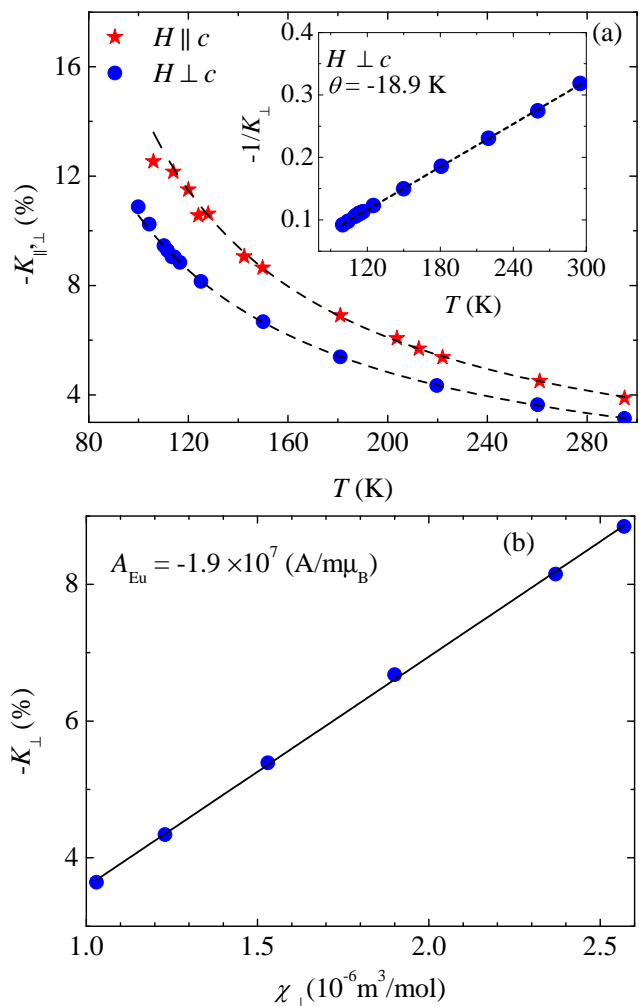


FIG. 6: (Color online) (a) Temperature dependence of the ^{75}As magnetic shift in a single crystal $\text{EuFe}_{1.9}\text{Co}_{0.1}\text{As}_2$ for $H \parallel c$ and $H \perp c$. The inset shows the inverse of the temperature dependent part of the shift $-1/K_{\perp}$ as a function of T . The dashed lines represent the Curie-Weiss behavior. (b) Plot of $-K_{\perp}$ vs. χ_{\perp} as obtained from the susceptibility measurements. The solid line is a linear fit.

the magnetic susceptibility measurements. This suggests that the Curie-Weiss part of the shift arises from the hyperfine coupling between the ^{75}As nuclei and the $\text{Eu}^{2+} 4f$ moments. The remaining constant part of the shift K_0 could be related to the coupling of ^{75}As with the itinerant 3d electrons in the Fe_2As_2 layer, including an orbital shift. However, the value of K_0 is a factor two smaller than the total ^{75}As magnetic shift reported for $\text{BaFe}_{1.8}\text{Co}_{0.2}\text{As}_2$.³⁶ The contribution of Eu to the magnetic shift K_{Eu} can be related to the susceptibility χ_{Eu} of the localized Eu 4f moments as follows:

$$K_{\text{Eu}} = \frac{A_{\text{Eu}}}{gN_A\mu_B} \chi_{\text{Eu}} \quad (5)$$

where A_{Eu} is the ^{75}As hyperfine coupling with the 4f moments, N_A and μ_B are the Avogadro number and Bohr magneton, respectively. Fig. 6b shows K_{\perp} versus χ_{\perp} with the temperature as an implicit parameter. From the linear fit of this data we can estimate a hyperfine coupling constant $A_{\text{Eu}} = -1.9 \times 10^7$ A/m per μ_B . This value of A is almost 60 times larger than the one reported for $\text{NdFeAsO}_{0.85}\text{F}_{0.15}$.⁴⁵ It is known that the '1111' compounds are more anisotropic than the '122' compounds.⁴⁶ Therefore, the '1111' systems are treated as quasi two-dimensional, while the '122' systems are regarded as three dimensional systems. Moreover, the distance between the rare-earth ion Eu^{2+} and the conduction layers in $\text{EuFe}_{1.9}\text{Co}_{0.1}\text{As}_2$ is $d = c/2 = 5.9713(3)$ Å, which is much smaller than in $\text{NdFeAsO}_{0.85}\text{F}_{0.15}$ ($d = 8.577$ Å).⁴⁵ The smaller interlayer distance in the '122' compounds as compared to the '1111' system and the more isotropic band structure may be the reason for the much stronger hyperfine coupling in the '122' compound. The large value of hyperfine coupling constant, quantitatively determined from the present NMR experiment, provides direct experimental evidence for a strong coupling between the Eu^{2+} localized moments and the $\text{Fe}_{1.9}\text{Co}_{0.1}\text{As}_2$ layers. This suggests that the magnetic exchange interaction between the localized Eu 4f moments is mediated by the itinerant Fe 3d electrons, *i.e.*, via a Ruderman-Kittel-Kasuya-Yosida (RKKY) type of mechanism^{19,28} leading to a high magnetic ordering temperature of the Eu^{2+} moments in EuFe_2As_2 . It was shown that Co-substitution induces superconductivity in $\text{EuFe}_{2-x}\text{Co}_x\text{As}_2$ with a reentrant behavior of resistivity due to the antiferromagnetic ordering of the Eu^{2+} spins.²³ Reentrant superconducting behavior was also observed in a EuFe_2As_2 crystal under an applied pressure up to 2.5 GPa.^{24,25} Moreover, while superconductivity with a maximum $T_c = 20$ K has been reported for $\text{BaFe}_{2-x}\text{Ni}_x\text{As}_2$,²⁹ no superconductivity was observed in $\text{EuFe}_{2-x}\text{Ni}_x\text{As}_2$.²⁸ The strong interaction between the localized Eu^{2+} moments and charge carriers in the $\text{Fe}_{2-x}\text{Co}_x\text{As}_2$ layers may cause pair breaking according to the Abrikosov-Gorkov theory,⁴⁷ which may be the reason why it is difficult to get superconductivity in $\text{EuFe}_{2-x}\text{Co}_x\text{As}_2$.

Finally, we would like to discuss the temperature de-

pendence of the resonance frequency and the skewness of a ^{75}As lower-satellite line for $H \perp c$ (see Fig. 7). A Change in the slope of the temperature dependence of the satellite line frequency can be seen at 225 K as shown in Fig. 7a. The inset of Fig. 7a illustrates a typical ^{75}As -NMR spectrum of the low-frequency satellite at 263 K. The spectra exhibit an asymmetric lineshape in the investigated temperature range. We analyzed the asymmetry of the satellite line shape at different temperatures by calculating its skewness (see Fig. 7b), defined as the third standardized moment. With decreasing temperature the skewness exhibits an increase down to 225 K, where it starts to reduce again. The slope change in the temperature dependence of the frequency of the ^{75}As lower-satellite line as well as the maximum in the temperature evolution of the skewness may be related to the appearance of an electronic nematic phase below 225 K in $\text{EuFe}_{1.9}\text{Co}_{0.1}\text{As}_2$. Note that evidence for an electron nematic phase transition was recently established in undoped AFe_2As_2 ($A=\text{Ba}, \text{Ca}$)⁴⁸ and Co-doped $\text{BaFe}_{2-x}\text{Co}_x\text{As}_2$ ⁴⁹ single crystals by means of in-plane anisotropy measurements of the electrical resistivity.

In order to get more quantitative NMR results for a possible nematic phase, the angular dependence of the full ^{75}As NMR spectrum (central line and both satellite

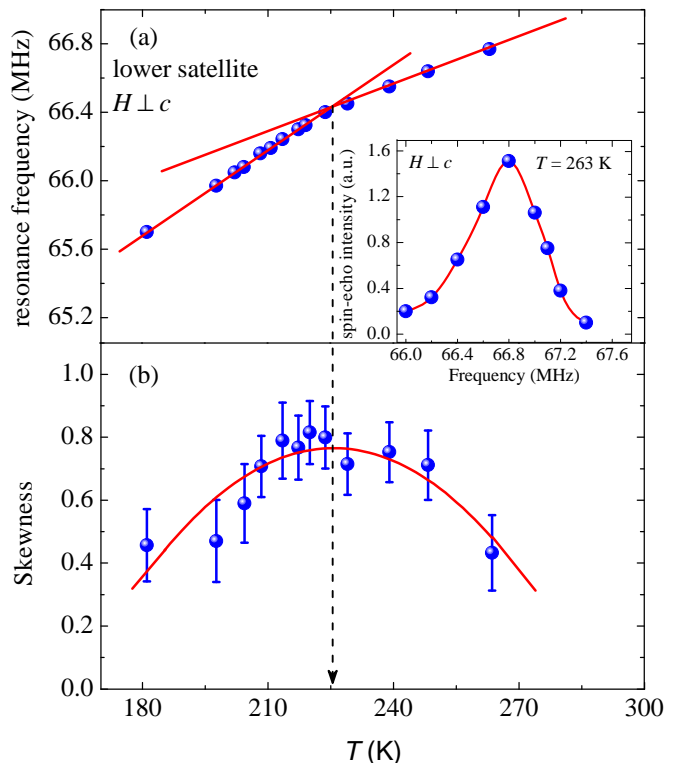


FIG. 7: (Color online) Temperature dependence of the frequency (a) and the skewness (b) of the ^{75}As lower-satellite line for $H \perp c$. The inset illustrates the ^{75}As NMR lower-satellite line shape at 263 K for $H \perp c$. Solid and dashed lines are guides to the eye.

lines) was measured at 181 K. The dominant contribution to the magnetic shift stems from the Eu^{2+} $4f$ moments (see above), and it is acceptable to assume that this contribution does not have a strong ab -anisotropy. Therefore, we reduced the parameter set to $K_a = K_b = K_{ab}$, K_c , ν_Q , and η . Analysis of the angular dependence of the full spectrum using the diagonalization of the Hamiltonian [Eq. (2)] yields $K_{ab} = -0.059(1)$, $K_c = 0.069(2)$, $\nu_Q = 7.51(17)$ MHz, and $\eta = 0.04(3)$. The change in ν_Q compared to the value $\nu_Q = 7.39(24)$ MHz obtained at 261 K in the tetragonal phase is small. The slight increase of η may reflect the lower symmetry of the As site in a possible nematic phase. However, further experiments are needed to clarify the presence of a nematic phase in $\text{EuFe}_{1.9}\text{Co}_{0.1}\text{As}_2$. Resistivity measurements on detwinned⁵⁰ single crystals could provide more information by probing the in-plane electronic anisotropy.

D. SUMMARY AND CONCLUSIONS

In summary, the magnetic properties of $\text{EuFe}_{1.9}\text{Co}_{0.1}\text{As}_2$ single crystal were investigated by X-ray diffraction, magnetization, and ^{75}As NMR experiments. It was found that the temperature dependence of the ^{75}As magnetic shift as well as the spin-spin relaxation rate follow a Curie-Weiss type behavior,

implying that the ^{75}As nuclei interact with the localized Eu $4f$ moments in the Eu layer. A large value of the hyperfine coupling constant between the ^{75}As nuclei and the Eu $4f$ moments suggests a strong coupling between the Eu and $\text{Fe}_{1.9}\text{Co}_{0.1}\text{As}_2$ layers. Due to such a strong interlayer coupling the antiferromagnetic interaction between the localized Eu^{2+} $4f$ moments is probably mediated by a Ruderman-Kittel-Kasuya-Yosida (RKKY) type interaction. Evidence for a SDW transition at 120 K was obtained from magnetic susceptibility as well as from ^{75}As -NMR measurements. A change of the slope in the temperature dependence of the frequency of the ^{75}As lower-satellite line is observed at 225 K. In addition, at the same temperature also a maximum in the temperature behavior of the skewness is detected. These findings may indicate a phase transition to an electron nematic state below 225 K.

IV. ACKNOWLEDGMENTS

This work was supported by the Swiss National Science Foundation, the SCOPES grant No. IZ73Z0.128242, the NCCR Project MaNEP, the EU Project CoMePhS, and the Georgian National Science Foundation grant GNSF/ST08/4-416.

-
- * Electronic address: zurabgug@physik.uzh.ch
- ¹ Y. Kamihara, T. Watanabe, M. Hirano, and H. Hosono, *J. Am. Chem. Soc.* **130**, 3296 (2008).
 - ² X.H. Chen, T. Wu, G. Wu, R.H. Liu, H. Chen, and D.F. Fang, *Nature (London)* **453**, 761 (2008).
 - ³ F. Chen, Z. Li, D. Wu, G. Li, W.Z. Hu, J. Dong, P. Zheng, J.L. Luo, and N.L. Wang, *Phys. Rev. Lett.* **100**, 247002 (2008).
 - ⁴ Z.A. Ren, J. Yang, W. Lu, W. Yi, G.C. Che, X.L. Dong, L.L. Sun, and Z.X. Zhao, *Mater. Res. Innovations* **12**, 105 (2008).
 - ⁵ Z.A. Ren, J. Yang, W. Lu, W. Yi, X.L. Shen, Z.C. Li, G.C. Che, X.L. Dong, L.L. Sun, F. Zhou, and Z.X. Zhao, *Europhys. Lett.* **82**, 57002 (2008).
 - ⁶ H.H. Wen, G. Mu, L. Fang, H. Yang, and X.Y. Zhu, *Europhys. Lett.* **82**, 17009 (2008).
 - ⁷ C. Wang, L.J. Li, S. Chi, Z.W. Zhu, Z. Ren, Y.K. Li, Y.T. Wang, X. Lin, Y.K. Luo, S. Jiang, X.F. Xu, G.H. Cao, and Z.A. Xu, *Europhys. Lett.* **83**, 67006 (2008).
 - ⁸ V. Johnson and W. Jeitschko, *J. Solid State Chem.* **11**, 161 (1974).
 - ⁹ P. Quebe, L.J. Terbüchte, and W. Jeitschko, *J. Alloys Compd.* **302**, 70 (2000).
 - ¹⁰ M. Pfisterer and G. Nagorsen, *Z. Naturforsch. B* **35B**, 703 (1980).
 - ¹¹ M. Pfisterer and G. Nagorsen, *Z. Naturforsch. B* **38B**, 811 (1983).
 - ¹² R. Marchand and W. Jeitschko, *J. Solid State Chem.* **24**, 351 (1978).
 - ¹³ G. Wu, H. Chen, T. Wu, Y.L. Xie, Y.J. Yan, R.H. Liu, X.F. Wang, J.J. Ying, and X.H. Chen, *J. Phys.: Condens. Matter* **20**, 422201 (2008).
 - ¹⁴ M. Rotter, M. Tegel, D. Johrendt, I. Schellenberg, W. Hermes, and R. Pöttgen, *Phys. Rev. B* **78**, 020503(R) (2008).
 - ¹⁵ C. de la Cruz, Q. Huang, J.W. Lynn, J. Li, W. Ratcliff II, J.L. Zarestky, H.A. Mook, G.F. Chen, J.L. Luo, N.L. Wang, and Pengcheng Dai, *Nature (London)* **453**, 899 (2008).
 - ¹⁶ Z.A. Ren, W. Lu, J. Yang, W. Yi, X.L. Shen, Z.C. Li, G. C. Che, X.L. Dong, L.L. Sun, F. Zhou, and Z.X. Zhao, *Chin. Phys. Lett.* **25**, 2215 (2008).
 - ¹⁷ S. Matsuishi, Y. Inoue, T. Nomura, M. Hirano, and H. Hosono, *J. Phys. Soc. Jpn.* **77**, 113709 (2008).
 - ¹⁸ J. Zhao, Q. Huang, C. de la Cruz, S. Li, J.W. Lynn, Y. Chen, M.A. Green, G.F. Chen, G. Li, Z. Li, J.L. Luo, N.L. Wang, and P. Dai, *Nature Materials* **7**, 953 (2008).
 - ¹⁹ H. Raffius, M. Mörsen, B.D. Mosel, W. Müller-Warmuth, W. Jeitschko, L. Terbüchte, and T. Vomhof, *J. Phys. Chem. Solids* **54**, 135 (1993).
 - ²⁰ Y. Xiao, Y. Su, M. Meven, R. Mittal, C.M.N. Kumar, T. Chatterji, S. Price, J. Persson, N. Kumar, S.K. Dhar, A. Thamizhavel, and Th. Brueckel, *Phys. Rev. B* **80**, 174424 (2009).
 - ²¹ A.S. Sefat, R. Jin, M.A. McGuire, B.C. Sales, D.J. Singh, and D. Mandrus, *Phys. Rev. Lett.* **101**, 117004 (2008).
 - ²² A. Leithe-Jasper, W. Schnelle, C. Geibel, and H. Rosner, *Phys. Rev. Lett.* **101**, 207004 (2008).
 - ²³ Y. He, T. Wu, G. Wu, Q.J. Zheng, Y.Z. Liu, H. Chen, J.J. Ying, R.H. Liu, X.F. Wang, Y.L. Xie, Y.J. Yan, J.K. Dong, S.Y. Li, and X.H. Chen, *J. Phys.: Condens. Matter*

- 22**, 235701 (2010).
- ²⁴ C.F. Miclea, M. Nicklas, H.S. Jeevan, D. Kasinathan, Z. Hossain, H. Rosner, P. Gegenwart, C. Geibel, and F. Steglich, *Phys. Rev. B* **79**, 212509 (2009).
- ²⁵ T. Terashima, M. Kimata, H. Satsukawa, A. Harada, K. Hazama, S. Uji, H.S. Suzuki, T. Matsumoto, and K. Murata, *J. Phys. Soc. Jpn.* **78**, 083701 (2009).
- ²⁶ Liling Sun, Jing Guo, Genfu Chen, Xianhui Chen, Xiaoli Dong, Wei Lu, Chao Zhang, Zheng Jiang, Yang Zou, Suo Zhang, Yuying Huang, Qi Wu, Xi Dai, Yuanchun Li, Jing Liu, and Zhongxian Zhao, *Phys. Rev. B* **82**, 134509 (2010).
- ²⁷ H.S. Jeevan, Deepa Kasinathan, H. Rosner, and P. Gegenwart, *Phys. Rev. B* **83**, 054511 (2011).
- ²⁸ Zhi Ren, Xiao Lin, Qian Tao, Shuai Jiang, Zengwei Zhu, Cao Wang, Guanghan Cao, and Zhuan Xu, *Phys. Rev. B* **79**, 094426 (2009).
- ²⁹ L.J. Li, Y.K. Luo, Q.B. Wang, H. Chen, Z. Ren, Q. Tao, Y.K. Li, X. Lin, M. He, Z.W. Zhu, G.H. Cao, and Z.A. Xu, *New J. Phys.* **11**, 025008 (2009).
- ³⁰ S. Jiang, Y.K. Luo, Z. Ren, Z.W. Zhu, C. Wang, X.F. Xu, Q. Tao, G.H. Cao, and Z.A. Xu, *New J. Phys.* **11**, 025007 (2009).
- ³¹ E. Dengler, J. Deisenhofer, H.A. Krug von Nidda, Seunghyun Khim, J.S. Kim, Kee Hoon Kim, F. Casper, C. Felser, and A. Loidl, *Phys. Rev. B* **81**, 024406 (2010).
- ³² J.J. Ying, T. Wu, Q.J. Zheng, Y. He, G. Wu, Q.J. Li, Y.J. Yan, Y.L. Xie, R.H. Liu, X.F. Wang, and X.H. Chen, *Phys. Rev. B* **81**, 052503 (2010).
- ³³ Kentaro Kitagawa, Naoyuki Katayama, Kenya Ohgushi, Makoto Yoshida, and Masashi Takigawa, *J. Phys. Soc. Jpn.* **77**, 114709 (2008).
- ³⁴ Kentaro Kitagawa, Naoyuki Katayama, Kenya Ohgushi, and Masashi Takigawa, *J. Phys. Soc. Jpn.* **78**, 063706 (2009).
- ³⁵ Fanlong Ning, Kanagasingham Ahilan, Takashi Imai, Athena S. Sefat, Ronying Jin, Michael A. McGuire, Brian C. Sales, and David Mandrus, *J. Phys. Soc. Jpn.* **77**, 103705 (2008).
- ³⁶ S.-H. Baek, N.J. Curro, T. Klimczuk, E.D. Bauer, F. Ronning, and J.D. Thompson, *Phys. Rev. B* **79**, 052504 (2009).
- ³⁷ APEX2 version 2009.9 (Bruker AXS Inc., 2009).
- ³⁸ SAINT version 7.68A (Bruker AXS Inc., 2009).
- ³⁹ XS version 2008/1 (George M. Sheldrick, *Acta Cryst.* (2008). A64, 112-122).
- ⁴⁰ XL version 2008/4 (George M. Sheldrick, *Acta Cryst.* (2008). A64, 112-122).
- ⁴¹ Shuai Jiang, Hui Xing, Guofang Xuan, Zhi Ren, Cao Wang, Zhu-an Xu, and Guanghan Cao, *Phys. Rev. B* **80**, 184514 (2009).
- ⁴² Z. Ren, Z.W. Zhu, S. Jiang, X.F. Xu, Q. Tao, C. Wang, C.M. Feng, G.H. Cao, and Z.-A. Xu, *Phys. Rev. B* **78**, 052501 (2008).
- ⁴³ N. Bloembergen and T.J. Rowland, *Acta Met.* **1**, 731 (1953).
- ⁴⁴ J. Winter, *Magnetic Resonance in Metals* (Oxford University Press, Oxford, 1971).
- ⁴⁵ P. Jeglič, J.-W. G. Bos, A. Zorko, M. Brunelli, K. Koch, H. Rosner, S. Margadonna, and D. Arčon, *Phys. Rev. B* **79**, 094515 (2009).
- ⁴⁶ Fengjie Ma, Zhong-Yi Lu, and Tao Xiang, *Front. Phys. China*, **5(2)**, 150 (2010).
- ⁴⁷ A.A. Abrikosov and L.P. Gor'kov, *Zh. Eksp. Teor. Fiz.* **39**, 1781 (1960) [*Sov. Phys. JETP* **12**, 1243 (1961)].
- ⁴⁸ M.A. Tanatar, E.C. Blomberg, A. Kreyssig, M.G. Kim, N. Ni, A. Thaler, S.L. Bud'ko, P.C. Canfield, A.I. Goldman, I.I. Mazin, and R. Prozorov, *Phys. Rev. B* **81**, 184508 (2010).
- ⁴⁹ Jiun-Haw Chu, James G. Analytis, Kristiaan De Greve, Peter L. McMahon, Zahirul Islam, Yoshihisa Yamamoto, and Ian R. Fisher, *Science* **329**, 824 (2010).
- ⁵⁰ M.A. Tanatar, A. Kreyssig, S. Nandi, N. Ni, S.L. Bud'ko, P.C. Canfield, A.I. Goldman, and R. Prozorov, *Phys. Rev. B* **79**, 180508(R) (2009).